

# Taxim: An Example-based Simulation Model for GelSight Tactile Sensors

Zilin Si<sup>1</sup> and Wenzhen Yuan<sup>1</sup>

**Abstract**—Simulation is widely used in robotics for system verification and large-scale data collection. However, simulating sensors, including tactile sensors, has been a long-standing challenge. In this paper, we propose Taxim, a realistic and high-speed simulation model for a vision-based tactile sensor, GelSight [1]. A GelSight sensor uses a piece of soft elastomer as the medium of contact and embeds optical structures to capture the deformation of the elastomer, which infers the geometry and forces applied at the contact surface. We propose an example-based method for simulating GelSight: we simulate the optical response to the deformation with a polynomial look-up table. This table maps the deformed geometries to pixel intensity sampled by the embedded camera. In order to simulate the surface markers’ motion that is caused by the surface stretch of the elastomer, we apply the linear elastic deformation theory and the superposition principle. The simulation model is calibrated with less than 100 data points from a real sensor. The example-based approach enables the model to easily migrate to other GelSight sensors or its variations. To the best of our knowledge, our simulation framework is the first to incorporate *marker motion field simulation* that derives from elastomer deformation together with the *optical simulation*, creating a comprehensive and computationally efficient tactile simulation framework. Experiments reveal that our optical simulation has the lowest pixel-wise intensity errors compared to prior work and can run online with CPU computing.

## I. INTRODUCTION

Simulation has been widely applied in robotics. For robotic tasks relying on vast amounts of data, simulation enables researchers to quickly generate large amounts of realistic data, without costly equipment, manual labour, and the risk associated with real-world experiments. With growing interest in robotics simulation, well-developed simulation frameworks such as PyBullet [2], MuJoCo [3], Drake [4], SOFA [5], NVIDIA Isaac Gym [6] have been widely used in the robotics community. They can simulate dynamic rigid-body, soft-body, vision and laser sensors with varying levels of accuracy and speed. However, none of them can simulate tactile sensors which form an irreplaceable part of robotic systems to capture local information such as contact forces [7], [8], shapes [9] and physical properties [10]. Recent advancements in vision-based tactile sensors, such as GelSight [11], [1], have made tactile sensing with high spatial resolution and speed possible. However, their designs, combining optical and soft-body components, make simulation challenging.

Vision-based tactile sensors like GelSight have a deformable soft pad, or *gelpad*, as the contact medium for

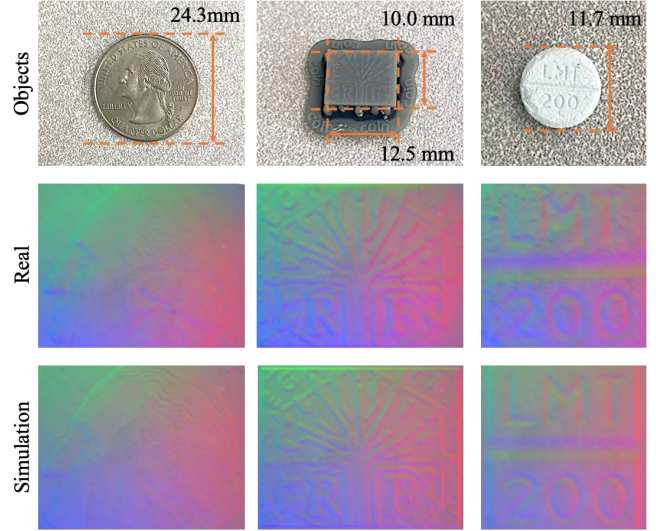


Fig. 1: The GelSight outputs when it contacts objects with rich textures. Using the ground-truth geometry, our simulation model generates images that are very similar to the real ones.

interacting with the environment. The printed marker array on the gelpad moves as the gelpad’s surface stretches and is a good indicator of the contact forces and torques. The sensor utilizes optical components, including LEDs to illuminate the gelpad and an embedded camera to capture the illumination change from contact geometries caused by the touching as shown in Fig 3. There have been previous studies on simulating different components of vision-based tactile sensors separately. For instance, Ding et al. [12] built a physics soft body simulation for the TacTip [13] sensor to indicate pins’ motion on the soft membrane; Agarwal et al. [14] and Gomes et al. [15] applied physics-based models for vision-based tactile optical simulation; whereas Wang et al. [16] integrated the optical simulation of tactile sensors with the physics simulation engine PyBullet. However, the work mentioned above are either limited by the lack of the ability to realistically simulate real world scenarios, the heavy computing demand, or hard to generalize to new sensors, which are balanced well in our work. We will show that our simulation is computationally lightweight and with small sim-to-real gap from experimental evaluation.

In this work, we propose Taxim, a tactile simulation model that combines *optical simulation* and *marker motion field simulation*. Our contributions are as follows:

- 1) We propose a polynomial table mapping function to

<sup>1</sup>Zilin Si and Wenzhen Yuan are with the Robotics Institute, Carnegie Mellon University, 5000 Forbes Ave, Pittsburgh, PA, 15213, USA <zsi, wenzheny>@andrew.cmu.edu

simulate the *optical response* of a GelSight sensor by mapping geometries to pixel intensity in tactile images and an accumulation approach to attach the shadow caused by the sensor design.

- 2) We develop a model to simulate the *marker motion field* using the soft-body linear elastic theory and the superposition principle for the gelpad’s elastic deformation.

Our simulation model is calibrated with less than 100 examples. This also enables our simulation model to easily migrate to other vision-based tactile sensors with similar designs as GelSight. To the best of our knowledge, Taxim is the first model that simulates all functions of vision-based tactile sensors, including the optical system for geometry measurement and marker motion field for force/torque measurement. We believe that our simulation model can be integrated into other simulation engines and provides a solid ground for the future manipulation research with tactile feedback in simulation environments.

## II. RELATED WORK

### A. Tactile Sensing Simulation

The majority of tactile sensors use a soft medium for contact where the measurement of its deformation can indicate the contact situation. Therefore the sensor simulation has been mostly focused on simulating the elastomer deformation. Traditionally, elastic soft body simulation is typically modelled with finite element methods (FEM) [17], mass-spring model [18], particles [19] or learning methods [20]. So to simulate tactile sensors that use soft medium, a traditional way is to build an approximation model of the soft bodies. Pezzementi et al. [21] and Moisio et al. [22] simulated the low dimension tactile sensor signals. However, they are not applicable to the high-resolution vision-based tactile sensors such as GelSight. Narang et al. [23] simulated a 3D Finite Element Model of the BioTac sensor [24] and high-resolution contact data in ANSYS. As an extension work, they presented the simulation model of BioTac in Issac [6] and a generative learning framework to project the deformation and tactile signal to latent spaces and synthesis the BioTac signals for new deformation in [25]. Sferrazza et al. [26] and Sferrazza et al. [27] simulated the contact force distribution applied on the soft surface with a learning model for a vision-based tactile sensor. In this work, we approximate the deformation of the soft medium on the GelSight sensor with pyramid Gaussian kernels which is a practical approximation with low-computing cost.

### B. Optical Simulation for Tactile Sensors

For vision-based tactile sensors like GelSight, optical simulation is essential as the illumination change indicates the geometry of the contacted objects. Agarwal et al. [14] built the GelSight optical components and applied ray tracing to simulate the tactile images. Gomes et al. [15] and Hogan et al. [28] used Phong’s model to simulate the reflection and illumination. Instead of building the physics models, we use a data-driven model to simulate the visual tactile

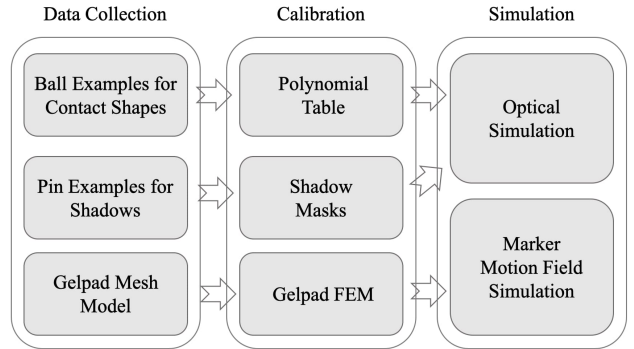


Fig. 2: The pipeline of our proposed example-based simulation model.

outputs and consider the optical features of the GelSight sensor such as area LED lights and spatial variance of the illumination. Wang et al. [16] presented TACTO, an open-source simulator for vision-based tactile sensors and bridged it to a physics simulator PyBullet. In this paper, we present our optical simulation model that can simulate high realistic tactile visual outputs in a computationally efficient way by comparing with aforementioned methods.

### C. Marker Motion Field Simulation for Tactile Sensors

The marker motion field refers to the movement of surface marker array caused by the surface stretch of the elastomer. In manipulation tasks such as slip detection [29] and grasping stability prediction [30], the marker motion field serves as an essential feature. For TacTip [13], a vision-based sensor with pins printed on the soft membrane, Ding et al. [12] simulated the dynamics of its soft membrane in Unity and extracted pins’ motion. They evaluated the simulation on sim-to-real tasks but lacked of the comparison between the simulated pin’s deformation with real data which is given quantitatively in our work. Besides the applied normal forces cases, we also consider the marker motion field under the shear loading which was not addressed in the above work. Church et al. [31] simulated the depth images to represent the contact geometries instead of optical tactile images with a Generative Adversarial Networks (GANs) for TacTip sensor. Unlike the above work, we explicitly simulate the marker motion field by applying FEM offline and using the superposition principle [32] online. Our method does not require extensive training data but it approximates the marker motion field well with high accuracy and low computation cost.

## III. METHODS

### A. Overview

We construct and employ our simulation models for both optical response and marker motion of the GelSight sensor. To simulate the sensor’s optical response, we build a polynomial table to map the contact geometries to the image intensities and collect shadow masks to attach the shadow. Then we apply the superposition principle based on the loading displacement of each finite unit to simulate the markers’ motion. Their combination replicates the contacting

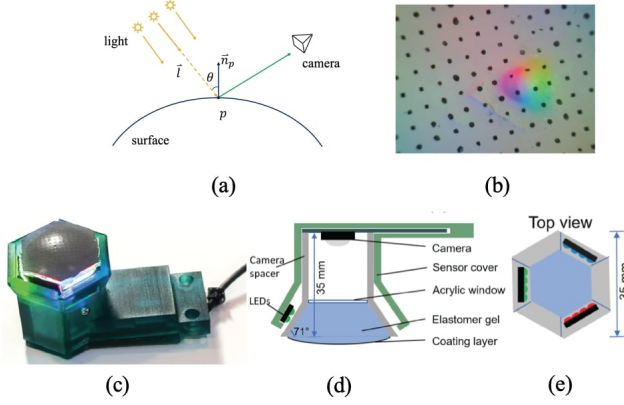


Fig. 3: (a) Demo of the photometric stereo method: for a surface point  $p$  under the light  $l$ , the reflected light intensity captured by the camera is determined by the surface reflectance and the surface normal  $\vec{n}_p$  (b) Outputs of the GelSight when in contact with a metal ball [33]. (c) The GelSight sensor [33] we aim to simulate. (d) and (e) show the schematic diagrams of the optical structure [33].

of objects on the tactile sensor. For both parts, we calibrate our simulator with examples from a real sensor. We show the pipeline for building and applying the simulation model in Fig. 2.

### B. Optical Simulation

We simulate the optical response of the GelSight sensor as a result of the contact geometry with a model using the examples-based photometric stereo [34] method. Photometric stereo uses the linear reflection function to derive the illumination of the object with the light sources and shape of the illuminated surface. Example-based photometric stereo does not require prior knowledge of lights sources but instead uses the imaging of the reference objects. We use a lookup table as the baseline and a polynomial table as our proposed method to map the contact shapes to image intensities.

*a) Lookup Table Mapping:* The gelpad has a homogeneous diffuse internal surface illuminated by LED lights which makes the reflection function invariant over the surface. The linear reflection function used by photometric stereo is formalized as  $I_p = \rho \mathbf{n}_p \sum \mathbf{l}$ , where given a point  $p$ , the observed intensity  $I_p$  from the reflection is a product of the albedo  $\rho$ , the surface shape  $\mathbf{n}_p$  and the light direction and intensity  $\mathbf{l}$ , as shown in Fig. 3 (a). The previous equation implies that the intensity  $I$  and the surface normal  $\mathbf{n}$  are linearly correlated. Alternatively, instead of solving the equation from the given lighting conditions, an intensity-shape lookup table can be built as follows

$$I = \sum_l a_l \mathbf{n} \quad (1)$$

where  $a_l$  as coefficients for the certain lights, can be calibrated from the examples similar to [11], [35]. Here, we consider that the light of the same color—any of red, green or blue—equates to one light source, even though they are made from multiple LEDs.

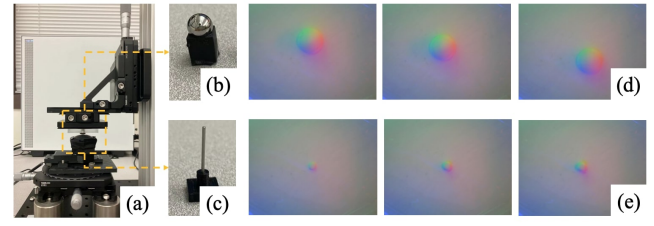


Fig. 4: Data collection setup (a, b, c) and data examples (d, e) to build the optical simulation model. The GelSight is placed on an XYR optical stage and an indenter with a certain shape object is mounted on a vertical linear stage for precisely indenting on the GelSight. We calibrate the polynomial table with 50 data points using a spherical indenter and collect shadow masks with 10 data points using a pin indenter.

*b) Polynomial Table Mapping:* The linear lookup table works well with the point lights which are far from the object, whose directions are parallel and intensities are uniform for all the points on the illuminated surface. However, the LED lights are grouped in arrays around the gelpad in the GelSight sensor, and as such, this assumption doesn't hold. Since the area LED lights cannot be approximated from the linear model precisely, we introduce a non-linear model for the reflection function as proposed in [36]. The reflection function can then be rewritten as

$$I = \sum_l f_{\mathbf{n}}^l(x, y) \quad (2)$$

where  $\mathbf{n}$  is the normal vector representative of the surface shape and  $(x, y)$  is the 2D location on the image plane. From experiments, we found that in practice a second order polynomial function is sufficient to approximate the non-linearity. Thus, the non-linear function is represented as:

$$f_{\mathbf{n}}^l(x, y) = ax^2 + by^2 + cxy + dx + ey + f \quad (3)$$

where  $(a, b, c, d, e, f)$  are parameters to model the polynomial table.

*c) Calibration:* Calibration entails fitting the parameters in the polynomial table from real data. Since these parameters vary for different sensors, this process has to be done per sensor. We use a metal ball with a known radius of 2mm in experiments to calibrate the parameters. During calibration, we press the ball over the surface and manually locate the circular region's center and radius in the tactile images as shown in Fig 4 (b) and (d). The normal direction of each point in the circular area can be calculated by comparing the radius in the image and the physical radius of the ball. We discretize the 3D normal vectors to a  $125 \times 125$  dimensional table in normal magnitude and normal direction. The parameters in polynomial table can then be solved via least squares with the set of intensity-shape-location pairs  $(I_p, \mathbf{n}_p, x_p, y_p)$  from collected data. We fill missing values in the table by interpolation.

*d) Simulation:* We simulate the visual outputs in three steps: collision detection, deformation approximation, and optical simulation. A collision is detected when an object comes in contact with the gelpad. From this contact, the local



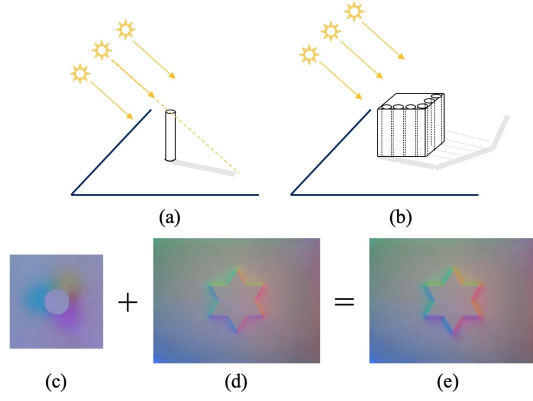


Fig. 5: Shadow synthesis. (a) A unit shadow case observed under the lighting. (b) To synthesis an object's shadow, we approximate the object as the composition of unit pin case and attach the shadow. (c), (d) and (e): We collect a set of shadow masks and attach the shadow to the contact area.

shape, represented as a height map, is constructed from the object's shape in the contact area, and gelpad's shape in non-contact area. Additionally, we need to simulate the soft body deformation from the height map. An approximation of soft body simulation is applied with pyramid Gaussian kernels. The shape in contact area is kept unchanged to maintain the contacting shape details and the boundaries between the contact and non-contact areas are smoothed using pyramid Gaussian kernels from large to small. From the height map, the normal vector for each point can be extracted and mapped to an intensity value with the calibrated polynomial table to synthesis the tactile images.

### C. Shadow Simulation

Other than the illumination change that is modeled with photometric stereo method, the shadow is another factor causing the change of the pixel intensity in the tactile images. According to the design of the sensor, the shadows are caused by three groups of LED lights: red, green and blue lights. Therefore we simulate the shadow from three light sources respectively.

Instead of tracking light beams in the space and generating the shadow on the illuminated surface, we simplify shadow casting by collecting the "unit" shadow case, and then simulate the shadow by accumulating the "unit" shadows. Since each light beam is assumed to be traveling independently in the space, without considering inter-reflection, the shadow cast by them can be linearly accumulated.

A "unit" shadow is the shadow of a standing pin as shown in Fig. 5 (a). For objects with different geometry, we can consider them as the accumulation of "unit" shadows placed side by side with different heights, as illustrated in Fig. 5 (b). Therefore, given the tactile images with casted shadow by indenting a pin normally onto the gelpad with different depths as shown in Fig. 4 (c) and (e), we extract a set of shadow masks on three dominant directions caused by three light sources. For a general case, the shadow mask is attached for all three color channels and all points within the contact area if the neighbors are lower than that point.

### D. Marker Motion Field Simulation

We simulate the markers' motion on the gelpad surface caused by the deformation of the soft gelpad from contacting. In this work, we consider the deformation under normal and shear loads. We employ the linear elasticity and superposition principle [32] to compose the deformation of the surface with loads on each finite unit of the contact surface. Although the markers are sparsely spread on the surface, we mesh the surface with dense nodes in simulation, track each node's motion and then locate the markers' motions. With the dense solution, the method can be applied to markers at any locations. Nodes in the gelpad surface mesh are classified into two categories: active nodes and passive nodes. The active nodes are those which come in contact with the object and being applied external forces and internal elastic forces; whereas passive nodes are those in non-contacted area which are only constrained by the internal elastic forces.

The linear elasticity theory assumes that the nodes can influence each other in a linear way. By considering two nodes  $n_i$  and  $n_j$  with displacement in 3D as  $\mathbf{u}_i$  and  $\mathbf{u}_j$ , the  $n_j$  can be passively influenced by  $n_i$  as  $\mathbf{u}_j = T_{n_j}^{n_i} \mathbf{u}_i$ , where  $\mathbf{u}_i$  is the active motion and  $T_{n_j}^{n_i}$  is a  $3 \times 3$  tensor representing the mutual influence. The superposition principle states that a node  $n_i$ 's displacement  $\mathbf{u}_i$  is an aggregation of all active nodes' influence to it. Assume we have active nodes  $K = \{k_1, k_2, k_3, \dots, k_m\}$ , where  $\mathbf{u}_i^k$  represent active nodes' displacement vector in 3D space. Under the linear elasticity theory and superposition principle, the influence of the active node  $k_i$  to other node  $n_j$  (including active nodes) can be represented as  $3 \times 3$  tensors  $T_{n_j}^{k_i}$  and each node's displacement can be composed as

$$\mathbf{u}_j = \sum_{i=1}^m T_{n_j}^{k_i} \mathbf{u}_i^k \quad (4)$$

However, before applying the superposition principle, we need to amend the active nodes' displacements because they are constrained to the load condition but also influence each other. For instance, if all the active nodes' displacements are initialized such that they only move along the  $z$  direction *i.e.*  $\mathbf{u}^k = [0, 0, dz]$ , and considering nodes are affected by other active nodes, then the following equation holds:

$$\mathbf{u}_j^k[z] = \sum_{i=1}^m T_{k_j}^{k_i}[3, 3] \tilde{\mathbf{u}}_i^k[z] \quad (5)$$

where  $\mathbf{u}_j^k$  is the initialized displacement, and  $\mathbf{u}_j^k[z]$  is its component along  $z$ -direction;  $\tilde{\mathbf{u}}_i^k$  is the virtual load displacement;  $T_{k_j}^{k_i}[3, 3]$  is the last element in the tensor  $T_{k_j}^{k_i}$ . Therefore, it is able to solve for virtual load displacement by stacking all the equations for active nodes as:

$$\mathbf{u}^k[z] = M_z \tilde{\mathbf{u}}^k[z] \quad (6)$$

$$\begin{bmatrix} \mathbf{u}_1^k[z] \\ \mathbf{u}_2^k[z] \\ \vdots \\ \mathbf{u}_m^k[z] \end{bmatrix} = \begin{bmatrix} T_1^1[3, 3] & T_1^2[3, 3] & \dots & T_1^m[3, 3] \\ T_2^1[3, 3] & T_2^2[3, 3] & \dots & T_2^m[3, 3] \\ \vdots & \vdots & \ddots & \vdots \\ T_m^1[3, 3] & T_m^2[3, 3] & \dots & T_m^m[3, 3] \end{bmatrix} \begin{bmatrix} \tilde{\mathbf{u}}_1^k[z] \\ \tilde{\mathbf{u}}_2^k[z] \\ \vdots \\ \tilde{\mathbf{u}}_m^k[z] \end{bmatrix}$$

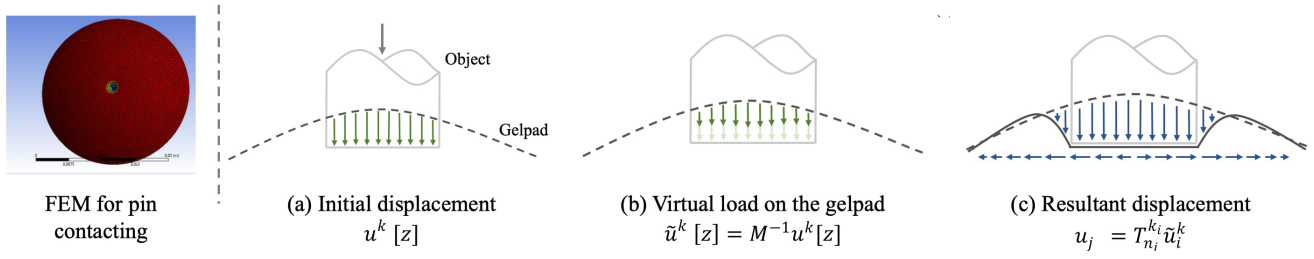


Fig. 6: Elastic deformation calibration and simulation for the gelpad. The unit pin with 0.5 mm diameter deformation case is simulated in ANSYS to get the dense nodal displacement results (left). In simulation, we apply the superposition principle to compose the displacement from the elastic deformation as (a) initial displacement boundary conditions, (b) active nodes' amended displacements, and (c) resultant nodal displacements.

Then  $\tilde{\mathbf{u}}^k[z]$  is solved by matrix inversion as  $\tilde{\mathbf{u}}^k[z] = M_z^{-1} \mathbf{u}^k[z]$ .

The  $x, y$  components of the active nodes' displacement can be amended using the same approach, but with  $T[1, 1]$  or  $T[2, 2]$  for the  $x$  or  $y$  directions respectively. Later, we apply the superposition principle to get the final resultant displacements for all nodes with

$$\mathbf{u}_j = \sum_i T_{n_j}^{k_i} \tilde{\mathbf{u}}_i^k \quad (7)$$

*a) Calibration:* The tensor  $T_{n_j}^{k_i}$  depends on the gelpad's physical properties, and therefore can be measured in advance. The markers on the real gelpad are sparsely distributed which can not be used to generate dense meshes. Instead, we calibrate the arbitrary  $T_{n_j}^{k_i}$  in a Finite Element Method (FEM) software ANSYS. In ANSYS, we generate the dense mesh of the gelpad and measure the deformation when there is a load on a unit node, as shown in Fig. 6 (left). We then use the measurement of the deformation to calibrate  $T$ . Since the markers are not printed on the top surface of the gelpad, we extract the second layer's mesh which is 0.5mm below the top surface from the simulated model as reference. To fully calibrate the  $3 \times 3$ -dimensional tensors, we simulate an active node's motion in z-direction only, a combination of z-direction and x-direction and a combination of z-direction and y-direction. Then we solve all the tensors  $T_{n_j}^{k_i}$  using least squares from these three sets of unit case.

*b) Simulation:* We employ the marker motion simulation in three steps, by: 1) applying the initial displacements on the active nodes, 2) amending the active nodes' displacements by superposition principle, and then 3) calculating the resultant displacements at each node using the superposition principle with the amended motions of the active nodes. This process is demonstrated in Fig. 6 (a), (b), (c).

#### IV. EXPERIMENTS

##### A. Experiment Setup and Data Collection

We set up an optical platform to collect data with a GelSight sensor. The GelSight is placed on the linear XYR stage, and an indenter is mounted on a vertical linear stage positioned above the GelSight, as shown in Fig. 4 (a). We manually control the contact location and depth by adjusting the stages so as to compare the simulated results with the real data. The XYR stage enables horizontal movement and

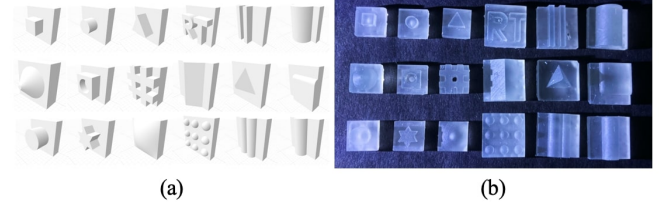


Fig. 7: Dataset of objects designed in Solidworks (a) and 3D printed (b) for contact experiments. The dataset includes objects with different shapes and textures. Objects are with the size 10mm  $\times$  10mm or 15mm  $\times$  15mm.

the vertical stage adjusts the indenting depth. Both are with 0.01mm graduation. We use the dome-shaped gelpad for both the real sensor and the simulated sensor.

We evaluate our simulation on a dataset that includes objects with different shapes and textures. The objects are designed in Solidworks [37], output as mesh files for simulation (Fig. 7 (a)) and 3D printed for collecting data from the real sensor for comparison (Fig. 7 (b)).

##### B. Optical Simulation

To calibrate the optical simulation model, we collect 50 data points on different locations of gelpad surface with a 4mm-diameter spherical indenter, as shown in Fig. 4 (b), (d); to calibrate the shadow simulation model, we collect 10 data points of different pressing depths with a 1mm-diameter pin indenter, as shown in Fig. 4 (c), (e).

We simulate the tactile images on the aforementioned dataset and compare our method with another three methods, physics-based model [14], TACTO [16] and Phong's model [15] as shown in Fig. 8. We evaluate our method by comparing the simulated images with the real images in pixel-wise level, against the three methods mentioned above on four metrics: mean absolute error (L1), mean squared error (MSE), structural index similarity (SSIM) and peak signal-to-noise ratio (PSNR). The simulated images are cropped to size 400  $\times$  400 around the indenting area to eliminate the background's effect. Also, due to the precision of the operation with the real sensor, the ground truth tactile images are not well aligned with the simulated images. So we manually align the images using GIMP [38]. The quantitative results are summarized in the Table. I. From the table, our method outperforms all the other methods.



Fig. 8: Optical simulation comparison among our method, TACTO [16], Phong [15] and physics [14] with the real data.

	L1 ↓	MSE ↓	SSIM ↑	PSNR ↑
Tacto [16]	10.861	215.861	0.808	25.495
Phong's [15]	8.163	123.249	0.832	27.763
Physics [14]	7.409	90.623	0.759	28.687
<b>Ours</b>	<b>5.565</b>	<b>58.358</b>	<b>0.882</b>	<b>30.974</b>

TABLE I: Image similarity metrics between simulated results and real data for optical simulation. We compare our method with methods from Physics-based model [14], Tacto [16] and Phong's model [15] on L1, MSE, SSIM and PSNR metrics. Our method performs the best on all the metrics.

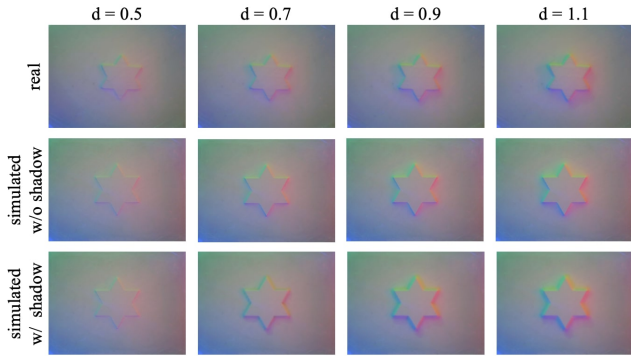


Fig. 9: Results for optical simulation with different indenting depths.

**Different Indenting Depth** Our optical simulation model works well for different indentation depths. One example is shown in Fig. 9.

**Spatial Variance** We compare our polynomial table with the lookup table to show that our method can handle the spatial variance over the camera's field of view. A metal sphere is pressed randomly on the gelpad illustrated as circles in Fig. 10 (a) and (b). Moreover, we interpolate the pixel-wised L1 errors as error maps shown in Fig. 10 (c) for polynomial table and (d) for the lookup table. The darker the color is, the larger the errors are. Error maps show that the lookup table has higher errors at the boundaries, but the

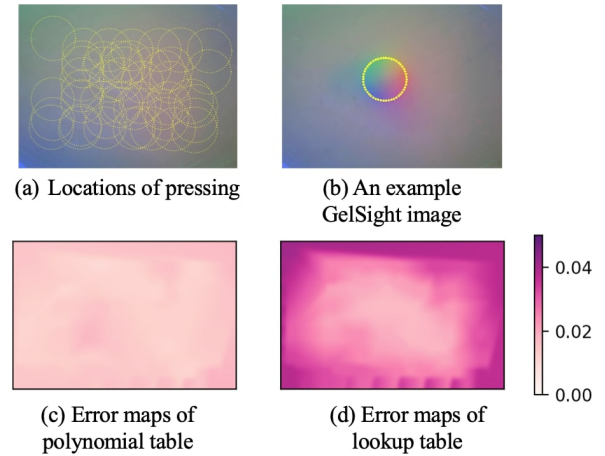


Fig. 10: Spatial distribution of simulation error when using the polynomial mapping method (c) and lookup table method (d). We compare the sphere's simulated tactile images with real tactile images where sphere is pressed at different locations as shown in (a) and (b), and the interpolated error maps are shown in (c) for polynomial mapping, (d) for lookup table.

polynomial table performs equally well over the different locations. Quantitatively, the polynomial table has 2.269 L1 intensities errors on average, while the lookup table has 5.590 in the range 0 to 255.

**Fine Texture Simulation** Our model can simulate the contact cases with fine-textured objects, as shown in Fig. 1.

**Speed Test** We test all the simulation techniques, mentioned above, on a AMD Ryzen Threadripper 2950X 16-Core Processor CPU. We input height maps with the size  $480 \times 640$ , and output the simulated tactile images of the dataset. We then record the average running time of all the methods, as shown in the Table II. Our method is the most



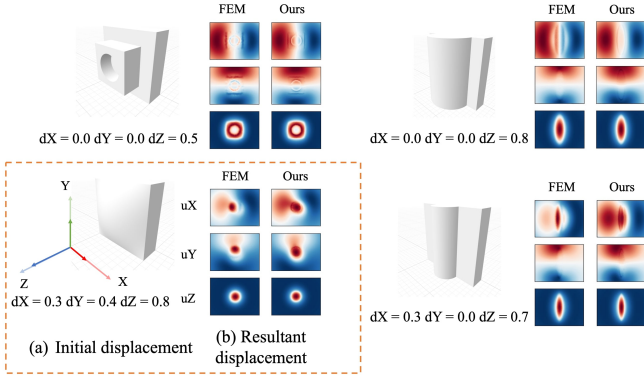


Fig. 11: The simulated marker motion field in a dense mesh in comparison with the FEM data. The heat maps show the marker motion field in X, Y and Z directions.

computational light-weighted on CPU. However, Tacto [16] and Physics model [14] can be largely accelerated on GPUs but not considered here for evaluation. Our method can be potentially optimized for GPU computation as well and we will work on that for the next step.

Speed	Ours w/o shadows	Ours w/ shadows	Physics [14]	Tacto [16]	Phong's [15]
Frequency (fps)	18.1	9.6	0.1	1.9	3.8

TABLE II: Speed test for optical simulation on CPU. We compare our method with the Physics-based model [14], Tacto [16] and Phong's model [15]. Our method runs with the fastest speed.

### C. Marker Motion Field Simulation

We evaluate the simulation results with two references: 1) the dense displacement map generated by the FEM simulation, and 2) the sparse displacement map collected from a real sensor. The contact cases are with objects in Fig. 7 under combinations of different normal loads and shear loads. The load displacement varies from 0.3 mm to 0.8 mm.

**Comparison between ANSYS simulation and our simulation** As illustrated in the four sets of comparison from Fig. 11, the dense mesh vertices displacements on X, Y, Z are simulated from both the FEM (Fig. 11 (b) left) and our methods (Fig. 11 (b) right). The color red means negative displacement value and blue means positive values. The average interpolated pixel-wised L1 errors over the gelpad surface on dataset are  $3.58 \times 10^{-3}$  mm for X-axis,  $3.32 \times 10^{-3}$  mm for Y-axis,  $5.43 \times 10^{-3}$  mm for Z-axis, and  $5.40 \times 10^{-3}$  mm for XY (gelpad surface).

**Comparison among real data, FEM simulation and our simulation** We also compare the nodal displacements amount the real data, FEM simulation, and our simulation. The mean of marker motion's magnitude L1 errors on dataset is  $1.00 \times 10^{-2}$  mm between real & FEM,  $1.02 \times 10^{-2}$  mm between real & ours, and  $3.96 \times 10^{-3}$  mm between FEM & ours. We weight the marker motion's angular errors based on the its magnitude because smaller marker motion is easier being affected by the system noise. The weighted mean of

marker motion's angular L1 errors is  $12.94^\circ$  between real & FEM,  $14.57^\circ$  between real & ours, and  $4.89^\circ$  between FEM & ours. From the experimental results, the FEM model and our model match well, but there is still a gap from the simulation to the real gelpad soft body model. Three reasons observed from the experiments causing the errors are: 1) The gelpad is hand-manufactured and it is not perfectly matched with the FEM model in ANSYS. 2) The marker motions tracked from the real sensor's data have the noise in marker extraction and tracking. 3) When shear loads present, our model cannot model the partial slip but it is very common for the real contact cases.

**Speed Testing** Our dense marker motion field simulation runs 9.22 seconds on average tested with CPU only. According to Narang et al. [25]'s 5.57 seconds per sim for BioTac sensor in Isaac Gym with GPU acceleration, our simulation has a reasonable low computing demand.

We show some final results that combine the optical simulation and marker motion simulation in Fig. 12.

## V. CONCLUSION

We present Taxim, an example-based GelSight tactile simulation model that combines optical and marker motion field simulation. We construct a polynomial table to simulate the optical response of GelSight from the contact geometry, and apply the linear elastic theory and the superposition principle to simulate the markers' motion. Our simulation is computationally light weight, easy to set up and use, and simple to apply to different sensors. It also incorporates the sensor's illumination features and system noise through calibration with examples from the real sensor. We have shown that our optical simulation outperforms the other state-of-the-art tactile simulations, and our marker motion field simulation achieves high accuracy by evaluating on a self-designed dataset. To the best of our knowledge, this is the first integrated work considering both the optical and marker motion simulation.

## REFERENCES

- [1] W. Yuan, S. Dong, and E. H. Adelson, "Gelsight: High-resolution robot tactile sensors for estimating geometry and force," *Sensors*, vol. 17, no. 12, p. 2762, 2017.
- [2] E. Coumans and Y. Bai, "Pybullet, a python module for physics simulation for games, robotics and machine learning," 2016.
- [3] E. Todorov, T. Erez, and Y. Tassa, "Mujoco: A physics engine for model-based control," in *2012 IEEE/RSJ International Conference on Intelligent Robots and Systems*, 2012, pp. 5026–5033.
- [4] R. Tedrake and the Drake Development Team, "Drake: Model-based design and verification for robotics," 2019. [Online]. Available: <https://drake.mit.edu>
- [5] J. Allard, S. Cotin, F. Faure, P.-J. Bensoussan, F. Poyer, C. Duriez, H. Delingette, and L. Grisoni, "Sofa-an open source framework for medical simulation," in *MMVR 15-Medicine Meets Virtual Reality*, vol. 125. IOP Press, 2007, pp. 13–18.
- [6] V. Makoviychuk, L. Wawrzyniak, Y. Guo, M. Lu, K. Storey, M. Macklin, D. Hoeller, N. Rudin, A. Allshire, A. Handa, et al., "Isaac gym: High performance gpu-based physics simulation for robot learning," *arXiv preprint arXiv:2108.10470*, 2021.
- [7] D. Ma, E. Donlon, S. Dong, and A. Rodriguez, "Dense tactile force estimation using gelsim and inverse fem," in *2019 International Conference on Robotics and Automation (ICRA)*. IEEE, 2019, pp. 5418–5424.

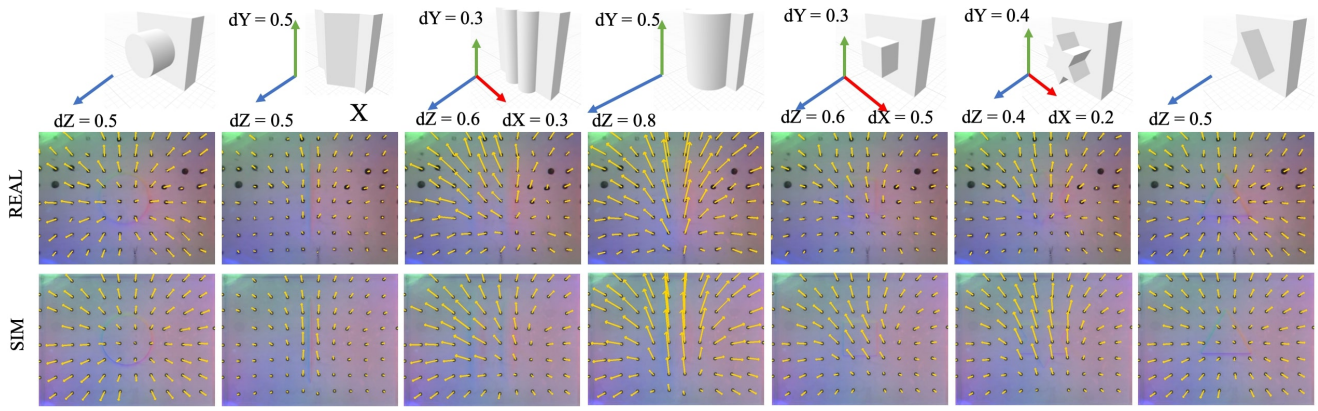


Fig. 12: Marker motion field simulation with optical simulation results. We visualize the marker motions (scaled up by 20 for better visualization) on the dataset under different normal displacements and shear displacements.

- [8] K. Sato, K. Kamiyama, N. Kawakami, and S. Tachi, "Finger-shaped gelforce: Sensor for measuring surface traction fields for robotic hand," *IEEE Transactions on Haptics*, vol. 3, no. 1, pp. 37–47, 2010.
- [9] M. Meier, M. Schopfer, R. Haschke, and H. Ritter, "A probabilistic approach to tactile shape reconstruction," *IEEE Transactions on Robotics*, vol. 27, no. 3, pp. 630–635, 2011.
- [10] W. Yuan, C. Zhu, A. Owens, M. A. Srinivasan, and E. H. Adelson, "Shape-independent hardness estimation using deep learning and a gelsight tactile sensor," in *2017 IEEE International Conference on Robotics and Automation (ICRA)*. IEEE, 2017, pp. 951–958.
- [11] M. K. Johnson and E. H. Adelson, "Retrographic sensing for the measurement of surface texture and shape," in *2009 IEEE Conference on Computer Vision and Pattern Recognition*, 2009, pp. 1070–1077.
- [12] Z. Ding, N. F. Lepora, and E. Johns, "Sim-to-real transfer for optical tactile sensing," in *2020 IEEE International Conference on Robotics and Automation (ICRA)*, 2020, pp. 1639–1645.
- [13] B. Ward-Cherrier, N. Pestell, L. Cramphorn, B. Winstone, M. E. Giannaccini, J. Rossiter, and N. F. Lepora, "The tactip family: Soft optical tactile sensors with 3d-printed biomimetic morphologies," *Soft robotics*, vol. 5, no. 2, pp. 216–227, 2018.
- [14] A. Agarwal, T. Man, and W. Yuan, "Simulation of vision-based tactile sensors using physics based rendering," *arXiv preprint arXiv:2012.13184*, 2020.
- [15] D. F. Gomes, P. Paoletti, and S. Luo, "Generation of gelsight tactile images for sim2real learning," *IEEE Robotics and Automation Letters*, vol. 6, no. 2, pp. 4177–4184, 2021.
- [16] S. Wang, M. Lambeta, P.-W. Chou, and R. Calandra, "Tacto: A fast, flexible and open-source simulator for high-resolution vision-based tactile sensors," *arXiv preprint arXiv:2012.08456*, 2020.
- [17] X. Wu, M. S. Downes, T. Goktekin, and F. Tendick, "Adaptive non-linear finite elements for deformable body simulation using dynamic progressive meshes," in *Computer Graphics Forum*, vol. 20, no. 3. Wiley Online Library, 2001, pp. 349–358.
- [18] F. Chen, L. Gu, P. Huang, J. Zhang, and J. Xu, "Soft tissue modeling using nonlinear mass spring and simplified medial representation," in *2007 29th Annual International Conference of the IEEE Engineering in Medicine and Biology Society*, 2007, pp. 5083–5086.
- [19] Y. Wang, W. Huang, B. Fang, and F. Sun, "Elastic interaction of particles for robotic tactile simulation," *arXiv preprint arXiv:2011.11528*, 2020.
- [20] D. Casas and M. A. Otaduy, "Learning nonlinear soft-tissue dynamics for interactive avatars," *Proceedings of the ACM on Computer Graphics and Interactive Techniques*, vol. 1, no. 1, pp. 1–15, 2018.
- [21] Z. Pezzementi, E. Jantho, L. Estrade, and G. D. Hager, "Characterization and simulation of tactile sensors," in *2010 IEEE Haptics Symposium*, 2010, pp. 199–205.
- [22] S. Moisio, B. León, P. Korkealaakso, and A. Morales, "Simulation of tactile sensors using soft contacts for robot grasping applications," in *2012 IEEE International Conference on Robotics and Automation*, 2012, pp. 5037–5043.
- [23] Y. S. Narang, K. Van Wyk, A. Mousavian, and D. Fox, "Interpreting and predicting tactile signals via a physics-based and data-driven framework," *arXiv preprint arXiv:2006.03777*, 2020.
- [24] T. Yamamoto, N. Wettels, J. A. Fishel, C.-H. Lin, and G. E. Loeb, "Biotac -biomimetic multi-modal tactile sensor," *Journal of the Robotics Society of Japan*, vol. 30, no. 5, pp. 496–498, 2012.
- [25] Y. Narang, B. Sundaralingam, M. Macklin, A. Mousavian, and D. Fox, "Sim-to-real for robotic tactile sensing via physics-based simulation and learned latent projections," *arXiv preprint arXiv:2103.16747*, 2021.
- [26] C. Sferrazza, A. Wahlsten, C. Trueeb, and R. D'Andrea, "Ground truth force distribution for learning-based tactile sensing: A finite element approach," *IEEE Access*, vol. 7, pp. 173 438–173 449, 2019.
- [27] C. Sferrazza, T. Bi, and R. D'Andrea, "Learning the sense of touch in simulation: a sim-to-real strategy for vision-based tactile sensing," in *2020 IEEE/RSJ International Conference on Intelligent Robots and Systems (IROS)*. IEEE, 2020, pp. 4389–4396.
- [28] F. R. Hogan, M. Jenkin, S. Rezaei-Shoshtari, Y. Girdhar, D. Meger, and G. Dudek, "Seeing through your skin: Recognizing objects with a novel visuotactile sensor," in *Proceedings of the IEEE/CVF Winter Conference on Applications of Computer Vision*, 2021, pp. 1218–1227.
- [29] W. Yuan, R. Li, M. A. Srinivasan, and E. H. Adelson, "Measurement of shear and slip with a gelsight tactile sensor," in *2015 IEEE International Conference on Robotics and Automation (ICRA)*, 2015, pp. 304–311.
- [30] R. Calandra, A. Owens, M. Upadhyaya, W. Yuan, J. Lin, E. H. Adelson, and S. Levine, "The feeling of success: Does touch sensing help predict grasp outcomes?" *arXiv preprint arXiv:1710.05512*, 2017.
- [31] A. Church, J. Lloyd, R. Hadsell, and N. F. Lepora, "Optical tactile sim-to-real policy transfer via real-to-sim tactile image translation," *arXiv preprint arXiv:2106.08796*, 2021.
- [32] S. Cotin, H. Delingette, and N. Ayache, "Real-time elastic deformations of soft tissues for surgery simulation," *IEEE Transactions on Visualization and Computer Graphics*, vol. 5, no. 1, pp. 62–73, 1999.
- [33] S. Dong, W. Yuan, and E. H. Adelson, "Improved gelsight tactile sensor for measuring geometry and slip," in *2017 IEEE/RSJ International Conference on Intelligent Robots and Systems (IROS)*. IEEE, 2017, pp. 137–144.
- [34] A. Hertzmann and S. Seitz, "Example-based photometric stereo: shape reconstruction with general, varying brdfs," *IEEE Transactions on Pattern Analysis and Machine Intelligence*, vol. 27, no. 8, pp. 1254–1264, 2005.
- [35] M. K. Johnson, F. Cole, A. Raj, and E. H. Adelson, "Microgeometry capture using an elastomeric sensor," *ACM Transactions on Graphics (TOG)*, vol. 30, no. 4, pp. 1–8, 2011.
- [36] M. Angelopoulou and M. Petrou, "Uncalibrated flatfielding and illumination vector estimation for photometric stereo face reconstruction," *Machine Vision and Applications*, vol. 25, pp. 1317–1332, 07 2014.
- [37] "Solidworks," <https://www.solidworks.com/>.
- [38] The GIMP Development Team, "Gimp." [Online]. Available: <https://www.gimp.org>